Light-Tunable Generation of Singlet Oxygen and Nitric Oxide with a Bichromophoric Molecular Hybrid: a Bimodal Approach to Killing Cancer Cells

Light-Tunable Generation of Singlet Oxygen and Nitric Oxide with a Bichromophoric Molecular Hybrid: a Bimodal Approach to Killing Cancer Cells

Aurore Fraix,[a] Marco Blangetti,[b] Stefano Guglielmo,[b] Loretta Lazzarato,[b] Nino Marino,[a] Venera Cardile,[c] Adriana C. E. Graziano,[c] Ilse Manet,[d] Roberta Fruttero,*[b] Alberto Gasco,[b] and Salvatore Sortino*[a]

Abstract: The design, synthesis, photochemical properties, and biological evaluation of a novel photoactivatable bichromophoric conjugate are reported. The compound **1**, [4-(4,4-difluoro-2,6-diiodo-1,3,5,7-tetramethyl-4-bora-3a,4a-diaza-s-indacen-8-yl)-N-(3-((4- nitro-3-(trifluoromethyl)phenyl)amino)propyl)butanamide] combines a 2,6-diiodo-1,3,5,7-tetramethyl BODIPY derivative as singlet oxygen ($^1O_2$) photosensitizer and 4-nitro-3-(trifluoromethyl) aniline (NOPD) as nitric oxide (NO) photodonor, joined by an alkyl spacer. These two chromogenic units absorb in distinct regions of the visible spectrum, and their individual photochemical properties are conserved in the molecular conjugate. Irradiation of the bichromophoric conjugate with green lightafforded $^1O_2$ in high quantum yields, whereas $^1O_2$ production was negligible with the use of blue light; under this latter condition, NO was released. Photogeneration of NO and cytotoxic $^1O_2$ can therefore be regulated by appropriately tuning the excitation light wavelength and intensity. Tested on melanoma cancer cells, this resulted in amplified photomortality relative to that of a structurally correlated model compound 2 [4-(4,4- difluoro-2,6-diiodo-1,3,5,7-tetramethyl-4-bora-3a,4a-diaza-s-indacen-8-yl)-N-(3-(p-tolylamino)propyl)butanamide] deprived of the NO-release capacity. The cellular uptake of **1**, evaluated by confocal fluorescence microscopy, showed that the product is localized in the cytoplasm.

Introduction

Photodynamic therapy (PDT) is a well-established therapeutic modality for treating malignant lesions, including cancer, in humans.[1, 2] PDT has some advantages over conventional therapies: it is noninvasive, selective, and repeated doses can be administered without initiating resistance.[3] PDT implies the combined use of a nontoxic photosensitizer (PS), low-energy light in the visible range, and molecular oxygen. It has generally been assumed that PDT, administered by the intravenous, intraperitoneal, or topical route, accumulates preferentially in tumor cells over normal cells, with a structure-dependent intracellular distribution.[2, 4] This preferential localization of the PS in tumor tissues is a very complex aspect of PDT, because the pharmacokinetic profile of a PS can vary dramatically with its structure, and can be modulated by using appropriate formulations.[5, 6] Illumination of the tumorous area with an appropriate dose of light of appropriate wavelength excites the PS, which reaches a lower-energy excited triplet state through intersystem crossing (ISC). The excited triplet state of the PS, which has a long lifetime, can be quenched by molecular oxygen via an electron and/or energy-transfer mechanism, giving rise to reactive oxygen species (ROS, Type II reaction), including the highly toxic singlet oxygen ($^1O_2$, Type I reaction).[4, 5, 7] The dynamic of the PS–oxygen interaction plays an important role in the efficacy of PDT.[8] ROS and $^1O_2$ are generated exclusively in the illuminated area, and are capable of inducing selective destruction of target tissues and cells through a number of mechanisms.[5, 7, 9] More recent results show that the oxidative stress induced by ROS also damages the tumor vasculature, with consequent formation of thrombogenic sites that induce ischemic death of the tumor tissue.[10] This effect is more efficient than killing tumor cells, and makes the endothelium the principal target for in vivo studies.[11] PDT can also be used for treating a variety of localized microbial infections. An advantage of this strategy is the eradication of chemotherapeutic-and antibiotic-resistant microorganisms, as well as of bacterial and fungal biofilms.[1, 12–14] Many PSs are currently being used in in vitro and in vivo studies; of these, porphyrinbased PSs are the most widely used.[15–18] Recently, derivatives of 4,4-difluoro-4-bora-3a,4a-diaza-s-indacene (BODIPY)[19–23] and their meso-aza analogues (aza-BODIPY)[24, 25] bearing appropriate substituents have emerged as an interesting new class of PSs, owing to their high extinction coefficients in the visible region, enhanced ISC quantum yields, long triplet lifetimes, and resistance to photobleaching.[23]

Nitric oxide (NO) is a ubiquitous gaseous messenger that plays a variety of roles in human physiology and pathophysiology. NO is involved in a number of biological processes, including vasodilation, platelet aggregation, neurotransmission, and macrophage-mediated immunity.[26] It has been suggested that NO may display its cytotoxic effects directly, for example, by inhibiting mitochondrial respiration and the citric acid cycle,[27] or indirectly, affording reactive nitrogen species (RNS) by reaction with oxygen and ROS. In particular, reaction of the superoxide anion ($O_2^{\cdot-}$) with NO generates peroxynitrite ($^-$OONO) which, in turn, affords two

very reactive and toxic radicals: $^{\cdot}OH$ and $^{\cdot}NO_2$.[28] It has also been suggested that NO can react with hydrogen peroxide to produce $^1O_2$.[27, 29] NO is involved in tumor biology and can display either stimulatory or inhibitory effects on cancer progression and metastasis, depending on several factors, in particular concentration, cellular sensitivity, and duration of exposure.[30–33] Great attention has thus been paid to molecular and macromolecular scaffolds able to release NO[34, 35] for potential therapeutic applications,[36, 37] including cancer.[38–40] An interesting class of NO donors are the NO photodonors (NOPDs): products which release NO under the action of light, and consequently allow very fine control of timing, location, and dosage of the NO released.[41] NOPDs must satisfy several prerequisites for bio-application, including excitation with visible light, and formation of nontoxic and nonvisible-light-absorbing side photoproducts. A major class of NOPDs are NO/nitrite complexes of transition metals combine with appropriate chromophores;[41b–d] their elaborate structures make them more difficult to manipulate than organic compounds, and carry some drawbacks due to the intrinsic toxicity of the metal center. Simple derivatives of nitroaniline, bearing a CF_3 substituent at the ortho position with respect to the nitro group, have proven to be organic NOPDs suitable for biological applications.[42–44] Like other nitrobenzene derivatives, their mechanism of NO release entails a nitro-to-nitrite photorearrangement, followed by release of NO with consequent formation of a phenol derivative.[45, 46] Furthermore, the simple structure of these NO photoprecursors makes them suitable for derivatization via simple synthetic procedures.[44] The combination of $^1O_2$ and NO provides a very appealing strategy in view of multimodal therapeutic systems. $^1O_2$ and NO share several important features, including: 1) small size and absence of charge, 2) capacity to attack different types of biological substrates (i.e., lipids, proteins, and DNA), 3) no multidrug resistance, 4) confinement of their action to short distances from the production site inside the cells (<20 nm for 1O2 and <200 mm for NO), due to their short lifetimes, decreasing systemic toxicity issues common to many conventional drugs. Furthermore, because NO photorelease is independent of O_2 availability, it successfully complements PDT at the onset of hypoxic conditions, typical for some tumors, where PDT may fail. In this framework, a multi-photoresponsive molecular hybrid, obtained by covalently joining a nitroaniline derivative NOPD with a porphyrin PS, was recently reported as potential anticancer drug.[47] Molecular conjugates in principle offer the great advantage of much more precise control over timing, location, and dosage of the cytotoxic species. In contrast to systems assembled by noncovalent interactions, which may suffer displacement in a biological environment, the covalent connection of the photoactive precursors ensures that the photodelivery events occur exactly in the “very same region of space” as the cell component. As further proof of this concept, the synthesis, spectroscopic and photochemical properties are here described of another prototype of this class, the molecular hybrid **1** (Scheme 1), obtained by linking 4-nitro-3-(trifluoromethyl) aniline NOPD with 2,6-diiodo-1,3,5,7-tetramethyl BODIPY as PS core through an appropriate spacer; its biological evaluation (cellular localization and cellular toxicity in/on A375 melanoma cells) is also reported. The model compound **2** (Scheme 1), lacking the NOPD unit but possessing hydrophobic-hydrophilic balance similar to **1**, was also considered for comparison.

Scheme 1. Structure of molecular conjugate **1** and model compound **2**.

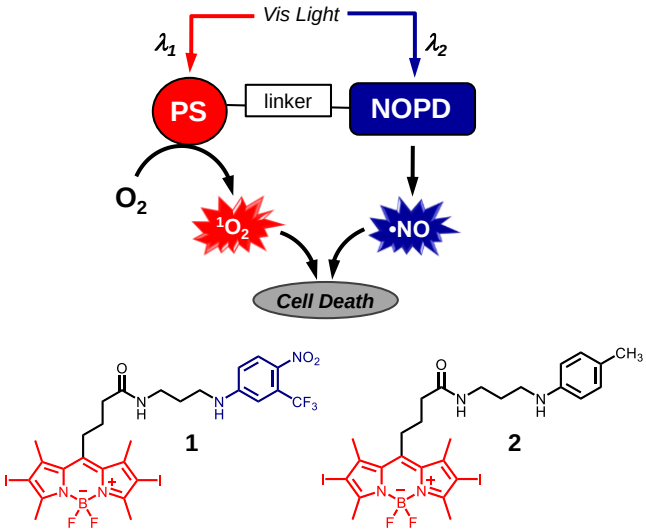

Results and Discussion

Design and synthesis

A specific point to be addressed in the fabrication of bimodal phototherapeutic systems exploiting the combined effects of $^1O_2$ and NO is the relative amounts of these cytotoxic species that are photogenerated: whereas $^1O_2$ is produced through a photophysical process that, in principle, does not consume the PS, photogeneration of NO implies a neat photochemical reaction with consequent degradation of the NOPD. As a result, in order to achieve effective bimodal performances, the multichromophoric nanoconstructs should be designed to avoid any spectral overlap of the absorption spectrum of the NOPD and that of the PS. In this case, the effect of $^1O_2$, photocatalytically generated in large amounts, could in principle mask the biological effects of NO to a significant extent, this conversely being produced through a photodecomposition pathway, in smaller quantities. Based on these considerations, the molecular hybrid **1** was designed and synthesized. Unlike porphyrin derivatives, whose Soret absorption bands overlap the absorption bands of the nitroaniline derivative NOPD to a considerable extent (at ~400 nm), the BODIPY chromophores strongly absorb beyond 500 nm, being basically transparent in the absorption spectrum of the NOPD. This design rationale should increase the performance of the resulting molecular hybrid, allowing fine tuning of the cytotoxic species by means of the appropriate selection of the light excitation wavelength and modulation of its intensity.

Compound **1** was synthesized by pathway A in Scheme 2. The BODIPY succinimidyl ester 3, already reported, was treated with N^1-(4-nitro-3-(trifluoromethyl)phenyl)propane-1,3-diamine **4** in a mixture of dichloromethane/DMF to give the expected adduct **5**. This intermediate was easily iodinated at the 2- and 6-positions by treatment with iodine and iodic acid to afford the desired final product **1**. A similar synthetic protocol was designed to prepare the model **2** (Scheme 2, pathway B). In this case iodination of the BODIPY core was initially carried out on the starting BODIPY butyric acid 6 to give 7. Coupling of the carboxylic acid 7 with N-hydroxysuccinimide (NHS) in the presence of N,N'-dicyclohexylcarbodiimide (DCC) then afforded the corresponding succinimidyl ester **8**. Final treatment of **8** with the anilino derivative **9**, under the conditions used to prepare intermediate **5**, yielded the target compound **2**.

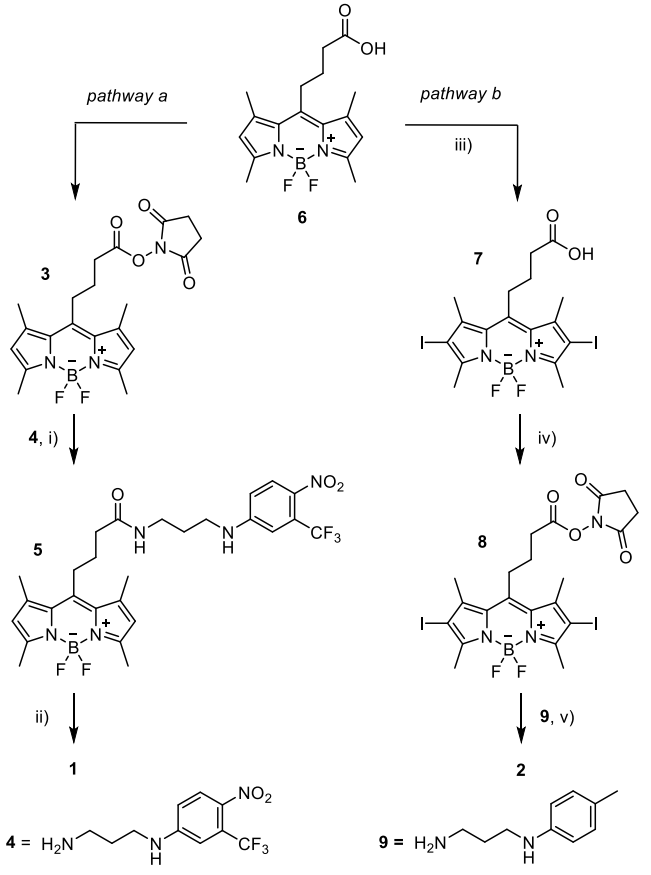

Scheme 2. Synthesis of compounds **1** (pathway A) and **2** (pathway B). Reagents and conditions: a) 4, dry CH_2Cl_2/DMF 1:1, RT, 1 h; b) I_2, HIO_3, EtOH, RT, 12 h; c) I_2, HIO_3, EtOH, RT, 30 min; d) NHS, DCC in dry CH_3CN/DMF 2:1, RT, 12 h; e) **9**, dry CH_2Cl_2/DMF 1:1, RT, 12 h.

Spectroscopic and photochemical properties

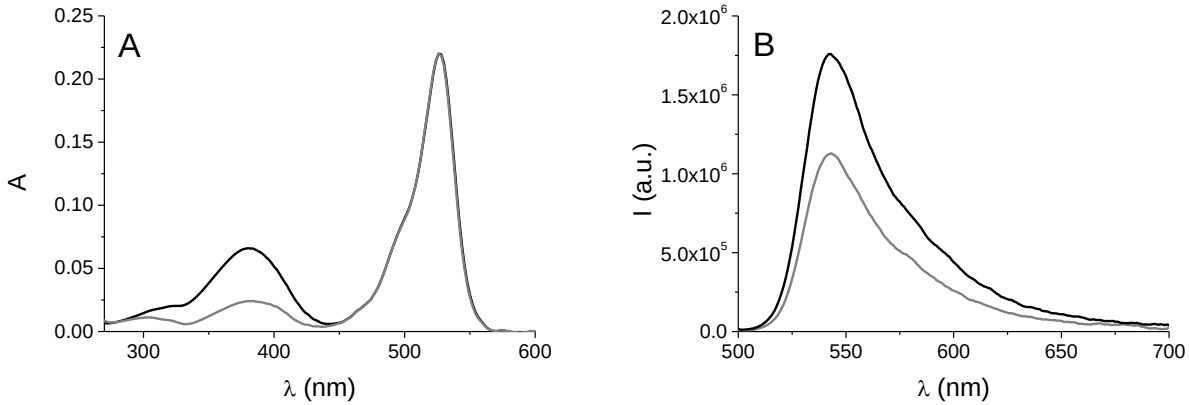

Figure 1. A) Absorption spectra of **1** (black) and **2** (grey) in acetonitrile. B) Fluorescence emission spectra (λ_{exc}=480 nm) of **1** (black) and **2** (grey) in acetonitrile. [**1**]= [**2**] = 6.5 μM.

Figure 1 shows the absorption and emission spectra of th conjugate **1** and the model compound **2** in acetonitrile solution. The characteristic absorption bands of the NOPD and BODIPY chromophores of **1** appear at 380 nm and 525 nm, respectively. The spectrum of model **2** presents the identical BODIPY band and a reduced absorbance in the 350–420 nm region due to the methyl aniline appendage. Compounds **1** and **2** exhibit similar fluorescence spectra with maxima centered at 542 nm, similar fluorescence quantum yields, being Φ_f=0.028 and Φ_f =0.020 for **1** and **2**, respectively, and very short fluorescence lifetimes, below 200 ps for both compounds. The low fluorescence quantum yields and the very fast fluorescence decay rates are perfectly in line with what has been observed for iodinated BODIPY derivatives[36] and is the result of the enhanced singlet-to-triplet ISC due to internal heavy-atom effect.

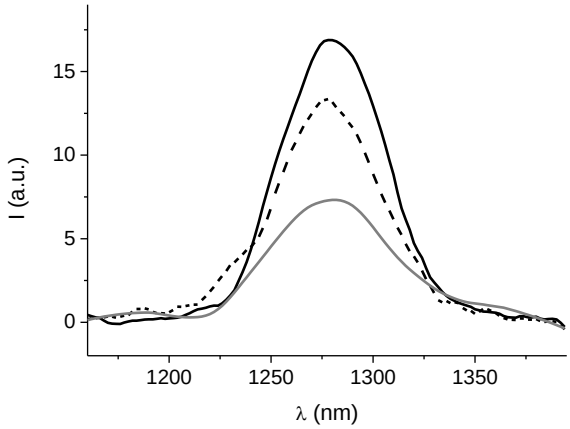

Figure 2. $^1O_2$ luminescence detected upon 524 nm light excitation of optically matched acetonitrile solutions of **1** (black), **2** (grey) and Rose Bengal (dashed).

$^1O_2$ production was detected directly and quantified by measuring its typical phosphorescence in the near-IR spectral window, upon excitation with green light. Figure 2 shows the luminescence signal observed for optically matched solutions of **1**, **2**, and Rose Bengal, this latter used as standard. Interestingly, the quantum yield for production of $^1O_2$ (Φ_Δ=0.78) for conjugate **1** is higher than that for the model compound **2** (Φ_Δ =0.48), showing that functionalization of the BODIPY core is compatible with the NOPD appendage in terms of $^1O_2$ photosensitization capability. This may be due to enhanced ISC efficiency in the case of **1**, as demonstrated by direct measurement of the excited triplet state of BODIPY, which is the precursor of $^1O_2$ (see below). In agreement with the spectral features of **1**, generation of $^1O_2$ was negligible, when the excitation light was commutated to the blue region (λexc=420 nm), where absorption by NOPD dominates over that by the BODIPY component.

Compounds **1** and **2** are insoluble in phosphate buffer solution, but present moderate solubility in culture medium (DMEM with 10% fetal calf serum (FCS) without phenol red) certainly due to the presence of proteins. The position of the absorbance bands (Figure 3a) is similar of those observed in acetonitrile. However, the band of the BODIPY chromophore is broader and undergoes hypochromism, probably due to a slight

aggregation phenomenon. Nevertheless, the emissive properties are not significantly different from those observed in organic solvent: although the fluorescence emission is broader and slightly blue-shifted (Figure 3b), the overall fluorescence quantum yields for **1** and **2** were very similar to those measured in acetonitrile.

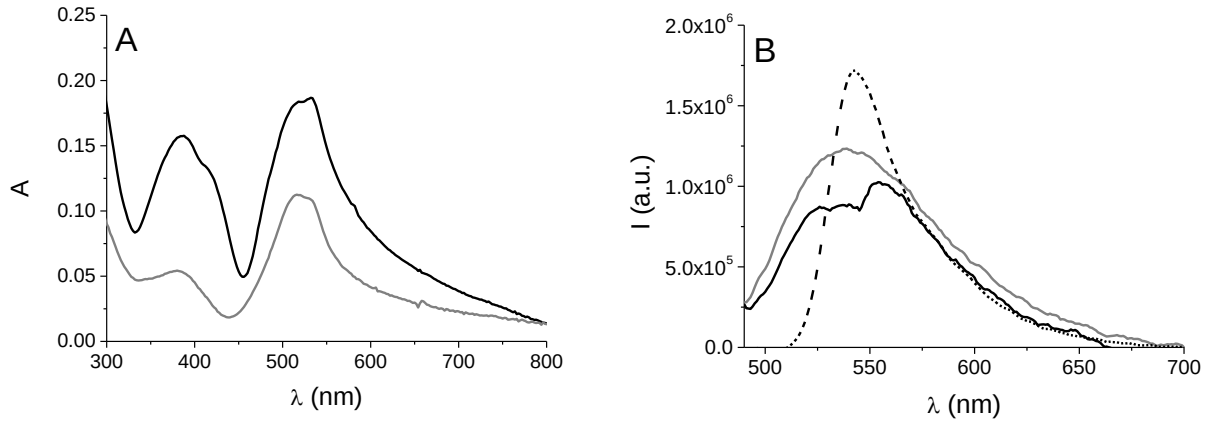

Figure 3. A) Absorption spectra of **1** (black) and **2** (grey) in culture medium. B) Fluorescence emission spectra (λ_{exc}=480 nm) of optically matched solutions of **1** (black) and **2** (grey) in culture medium and, for comparison, **1** in acetonitrile (dashed).

The excited triplet state of the BODIPY is the key transient intermediate for photosensitization of $^1O_2$, and its effective generation is thus crucial for photodynamic action to occur.[48]
Laser flash photolysis with nanosecond time-resolution is a powerful tool that can be used to examine the spectroscopic and kinetic features of excited triplets of many PSs, as these transient species exhibit very intense absorption in the visible region, and lifetimes in the order of microseconds. Figure 4 shows the transient absorption spectrum of compound **1** observed 0.1 ms after the laser pulse in culture medium and, for comparison, in acetonitrile solution. Both spectra show maxima at ~440 nm and bleaching at ~530 nm, in the region corresponding to the ground state absorption of the BODIPY chromophore, in line with the typical triplet state absorption of BODIPY derivatives.[33] In both solutions, the triplet state of **1** decays mono-exponentially (inset Figure 4) with a lifetime in culture medium of ~50 ms, almost one order of magnitude longer than that in the organic solvent. This sort of lifetime increase occurs quite commonly upon incorporation of chromophores into biological media or protein hosts, and is usually caused by the protection exerted by the host against external quenching impurities, or to a perturbation of the ISC process to the ground state, or to both.[49] This spectroscopic and kinetic scenario is similar to those observed with model compound **2**. However, in this case it was observed that the relative efficiency of population of the triplet state (Φ_T) was ~30% lower than that of **1** (see Experimental Section). This finding explains the lower quantum yield of $^1O_2$ observed for model compound **2** (see above). Selected photophysical properties of compounds **1** and **2** are summarized in Table 1.

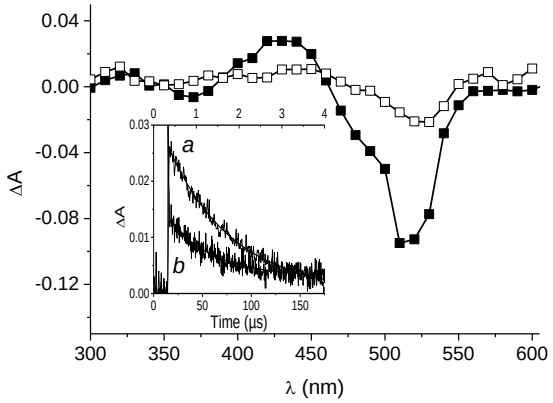

Figure 4. Transient absorption spectra observed 0.1 μs after 532 nm laser excitation (E_{532} ≈ 10 mJ/pulse) of optically matched N_2-saturated solution of **1** in acetonitrile (■) and in culture medium (□). The inset shows the decay traces monitored at 440 nm and the related first-order fitting of **1** in acetonitrile (*a*, X axes on top) and in culture medium (*b*, X axes on bottom).

Table 1. Selected photophysical properties of compounds **1** and **2** in ACN

	1	**2**
λ_{abs} (nm)	525 (max)	525 (max)
λ_{em} (nm) [a]	542	542
ε (M^{-1} cm^{-1})	48.000	48.000
Φ_f [b]	0.028	0.020
Φ_Δ [c]	0.78	0.48
τ^0_f (ps)	< 200	< 200
τ^1_T (µs)	1.5	1.8
Φ_T[d]	1	0.72

[a] λ_{exc}=480 nm. [b] Fluorescence quantum yields were determined using a solution of Fluorescein in EtOH as standard (Φ_f = 0.79). [c] $^1O_2$ quantum yields were determined using a solution of Rose Bengal in acetonitrile as standard (Φ_Δ = 0.65). [d] Relative Φ_T normalized with respect compound **1**.

The NO photorelease properties of the conjugate **1** were demonstrated by direct real-time monitoring using an ultrasensitive NO electrode, which directly detects NO with nanomolar concentration sensitivity by an ultrasensitive NO electrode employing an amperometric technique. The results illustrated in Figure 5 provide evidence that **1** is stable in the dark, and that it releases NO in a photoregulated fashion upon 405 nm light excitation. In agreement with the spectral features of, no photorelease of NO was observed when the excitation light was switched from 405 nm into the green region at 532 nm, where the BODIPY is the only absorbing chromophore.

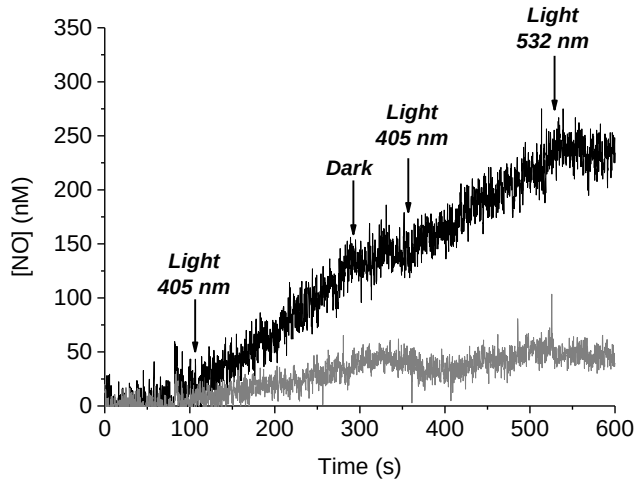

Figure 5. NO release profiles observed upon irradiation of solutions of **1** (black) and **2** (grey) in culture medium. [**1**]= [**2**]= 8.6 µM.

Cell internalization and viability assay

Compounds **1** and **2** were evaluated biologically by means of in vitro experiments on A375 cells, a human amelanotic melanoma cell line. The cellular uptake of **1** was determined by confocal fluorescence microscopy after 4 h incubation of a suspension in DMEM. Figure 6 shows the confocal fluorescence images of the melanoma cells treated with **1**, and excited at 405 nm and 488 nm, respectively. The 425–475 nm blue emission in the nucleus is due to DAPI fluorescence observed upon excitation at 405 nm, while the emission in the 500–550 nm green channel is due to the molecular hybrid 1. The typical BODIPY green fluorescence was noted in the cell cytoplasm, where it was also present in the form of aggregates. Results were similar for the model compound, reflecting the hydrophobic-hydrophilic balance of its molecular structure, very similar to **1**.

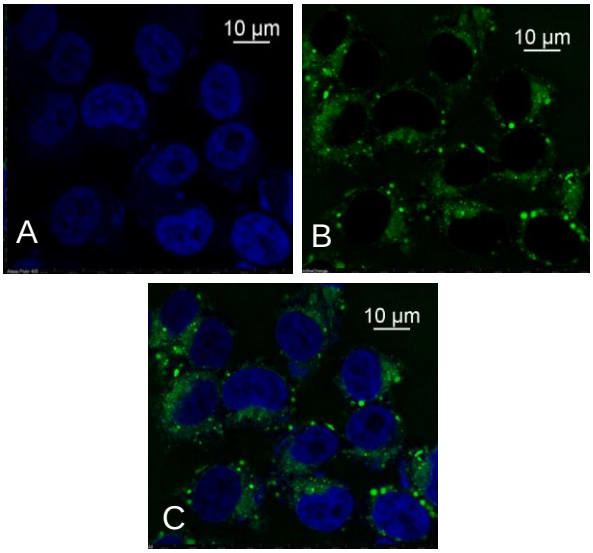

Figure 6. Evaluation of A375 cellular uptake of **1** by confocal fluorescence microscopy imaging. A and B are blue and green images for excitation at 405 and 488 nm, collecting fluorescence in the range 425–475 and 500–550, respectively. C) Merged images. [**1**]=[**2**]=10 µM

To validate the feasibility of the molecular conjugate as a bimodal phototherapeutic agent, the melanoma carcinoma cells were incubated with **1** or **2**, and either kept in the dark or irradiated simultaneously with blue and green light. In view of the photocatalytic generation of $^1O_2$ by the BODIPY, the green light source was adjusted so that it was more than one order of magnitude less intense than the blue light, which triggers NO generation non-catalytically through photodecomposition of the NOPD. Cell cytotoxicity was determined by MTT assay 4 h after completion of irradiation. The results in Figure 7 account for the very low cytotoxicity of both **1** and **2** in the dark. In contrast, marked cell mortality occurred under illumination. In particular, the extent of photomortality induced by **1** was significantly greater than that observed for the model compound **2**, this difference being greater at the longer irradiation time. Note that the larger photomortality induced by 1 is not the result of the high Φ_Δ value displayed by this compound if compared with the model **2** (see above). Rather, these findings provide clear-cut evidence for the involvement of a bimodal photo-inactivation mechanism in neoplastic destruction, in which the simultaneous release of cytotoxic NO and $^1O_2$ is envisaged to play a key role. Accordingly, the extent of the bimodal effect was decreased significantly as the intensity of the green excitation light increased (see Figure S1, Supporting Information). This is due to the much higher concentration of the photocatalitically produced $^1O_2$, the cytotoxic effect of which dominates over that of NO.

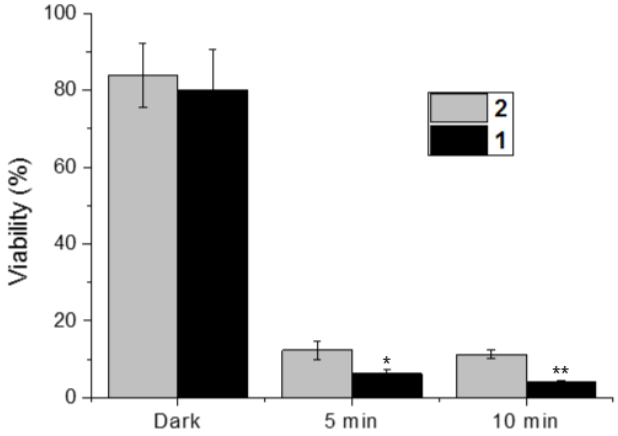

Figure 7. Cell viability of A375 melanoma cells incubated 1h with **1** and **2** and either kept in the dark or irradiated for 5 min and 10 min with simultaneous blue light (420 nm ≈ 7 mW cm^{-2}) and green light (528 nm ≈ 0.5 mW cm^{-2}) [**1**]= [**2**]= 10 µM. The significance of **1** vs **2** at 5 min: *p < 0.002, the significance of **1** vs **2** at 10 min: **p<0.001.

Conclusions

A novel photoactivable bichromophoric conjugate that can kill cancer cells by bimodal photoaction due to the light-triggered generation of ROS and RNS has been developed. The design rationale underlying this compound ensures not only the photochemical independence of the two light-harvesting units, but also their distinct excitation, by appropriately tuning the excitation light energy. NO and $^1O_2$ can be selectively or simultaneously photogenerated by using blue and/or green light. This affords accurate regulation of the relative concentrations of the two cytotoxic species, by appropriately modulating theintensities of the blue and green light excitation sources. This molecular hybrid thus represents a significant step forward over molecular conjugates combining the same NOPD and porphyrin PSs,[47] in which the considerable overlap of the absorption spectra of the two chromophores in the blue region seriously limits control over the relative amounts of $^1O_2$ and NO released. Studies on a wide series of these BODIPY–NOPD conjugates are currently in progress in the authors' laboratories, and the results will be reported in due course.

Experimental Section

Materials and methods

All reactions involving air-sensitive reagents were performed under nitrogen in oven-dried glassware using the syringe-septum cap technique. All solvents were purified and degassed before use. Chromatographic separation was achieved under pressure on Merck silica gel 60 using flash-column techniques. Reactions were monitored by thin-layer chromatography (TLC) on 0.25 mm silica gel coated aluminum plates (Merck 60 F_{254}) using UV light (254 nm) as visualizing agent. Unless otherwise specified, all reagents were used as received without further purification. CH_2Cl_2 was dried over P_2O_5 and freshly distilled under nitrogen prior to use. DMF was stored over 3 Å molecular sieves. Anhydrous CH_3CN was dried over CaH_2 and freshly distilled under nitrogen. ^{1}H NMR and ^{13}C NMR spectra were recorded at room temperature at 300 and 75 MHz, respectively, and calibrated using $SiMe_4$ as internal reference. Chemical shifts (δ) are given in parts per million (ppm), and coupling constants (J) in Hertz (Hz). The following abbreviations are used to designate the multiplicities: s=singlet, d=doublet, t=triplet, q=quartet, quint=quintet, m=multiplet, br=broad. Low-resolution mass spectra were recorded on a Micromass Quattro microTM API (Waters Corporation, Milford, MA, USA). Highresolution mass spectra were recorded on a Bruker Bio Apex Fourier transform ion cyclotron resonance (FT-ICR) mass spectrometer equipped with an Apollo I ESI source, a 4.7 T superconducting magnet, and a cylindrical infinity cell (Bruker Daltonics, Billerica, MA, USA). The purity of final compounds was determined by analytical HPLC analyses on Merck LiChrospher C18 end-capped column (250×4.6 mm ID, 5 mm) using CH_3CN/H_2O as solvent mixtures. BODIPYs **3** and **6**,[50] anilines **4**[51] and **9**[52] were synthesized by following reported procedures.

Synthesis

*4-(4,4-Difluoro-1,3,5,7-tetramethyl-4-bora-3a,4a-diaza-s-indacen-8-yl)-N-(3-((4-nitro-3-(trifluoromethyl)phenyl)amino)propyl)butanamide(**5**).* A solution of 4-(4,4-difluoro-1,3,5,7-tetramethyl-4- bora-3a,4a-diaza-s-indacene-8-yl)-butyric acid succinimidyl ester 3 (95 mg, 0.22 mmol) in dry CH_2Cl_2/DMF (1:1, 15 mL) under nitrogen was treated with N^1-(4-nitro-3-(trifluoromethyl)phenyl)propane-1,3- diamine **4** (58 mg, 0.22 mmol). The reaction mixture was stirred for 1 h at room temperature and the solvent removed under reduced pressure. EtOAc (30 mL) was added to the residue, which was washed with H_2O (3×10 mL), brine (2×10 mL), dried over Na_2SO_4 and concentrated to dryness. Purification by silica gel chromatography eluting with 98:2 $CHCl_3$/MeOH gave **5** as an orange solid (R_f=0.20, 89 mg, 70%); mp: (hexane/EtOAc)=196.6–199.8 °C; ^{1}H NMR (300 MHz, [D_6]DMSO): δ=8.05 (d, J=9.1 Hz, 1H), 8.01 (t, J=5.4 Hz, 1H), 7.55 (t, J=5.2 Hz, 1H), 7.04 (s, 1H), 6.80 (dd, J=9.2, 2.3 Hz, 1H), 6.21 (s, 2H), 3.26–3.12 (m, 4H), 2.98–2.87 (m, 2H), 2.39 (s, 12H), 2.29 (t, J=6.8 Hz, 2H), 1.85–1.65 ppm (m, 4H); ^{13}C NMR (75 MHz, [D_6]DMSO): δ=171.3, 156.6, 153.2, 146.3, 141.0, 133.5, 130.8, 129.8, 124.9 (q, J=32.2 Hz, 1C), 122.6 (q, J=272.4 Hz, 1C), 120.8, 111.8 (br, 2C), 40.4, 36.3, 35.5, 28.1, 27.6, 27.2, 15.8, 14.1 ppm; ESI-MS $[M+Na]^+$: m/z 602.0.

4-(4,4-Difluoro-2,6-diiodo-1,3,5,7-tetramethyl-4-bora-3a,4adiaza-s-indacen-8-yl)-N-(3-((4-nitro-3-(trifluoromethyl)phenyl)- amino)propyl)butanamide (**1**). A solution of compound **5** (30 mg, 0.052 mmol) in EtOH (30 mL) was treated with iodine (26.4 mg, 0.104 mmol) followed by iodic acid (18.3 mg, 0.104 mmol) in 2 mL H_2O. The reaction mixture was stirred overnight at room temperature and the solvent removed under reduced pressure. Purification by silica gel chromatography eluting with 96:4 CH_2Cl_2/MeOH gave 1 as a bright-red solid (R_f=0.40, 34 mg, 83%); mp: (hexane/ EtOAc)=185.2–186.6 °C (dec.); ^{1}H NMR (300 MHz, $CDCl_3$): δ=8.02 (d, J=9.1 Hz, 1H), 6.91 (s, 1H), 6.64 (d, J=9.1 Hz, 1H), 3.31 (t, J= 6.6 Hz, 2H), 3.23 (t, J=6.0 Hz, 2H), 3.14–3.04 (m, 2H), 2.61 (s, 6H), 2.49 (s, 6H), 2.37 (t, J=6.9 Hz, 2H), 2.02–1.88 (m, 2H), 1.86– 1.72 ppm (m, 2H); ^{13}C NMR (75 MHz, $CDCl_3$): δ=173.3, 155.7, 152.8, 145.3, 142.7, 135.5, 131.6, 129.6, 126.8 (q, J=33.1 Hz, 1C), 122.6 (q, J=273.0 Hz, 1C), 112.0, 111.6–111.0 (m, 1C), 86.7, 40.3, 37.0, 36.0, 29.8, 28.5, 27.5, 19.0, 16.2

ppm; ESI-HRMS $[M+H]^+$: 832.0445, $C_{27}H_{30}BF_5I_2N_5O_3$ requires 832.0450; HPLC purity .95% (CH_3CN/H_2O HCOOH 0.1% 80:20 (v/v), flow=1.5 mLmin^{-1}, t_R=11.4 min) at 226, 254, 420 and 540 nm.

4-(4,4-Difluoro-2,6-diiodo-1,3,5,7-tetramethyl-4-bora-3a,4adiaza- s-indacene-8-yl)-butyric acid (**7**). A solution of 4-(4,4-difluoro- 1,3,5,7-tetramethyl-4-bora-3a,4a-diaza-s-indacene-8-yl)-butyric acid **6** (169 mg, 0.506 mmol) in EtOH (40 mL) was treated with iodine (321 mg, 1.26 mmol) followed by iodic acid (222 mg, 1.26 mmol) in 5 mL H_2O. The reaction mixture was stirred at room temperature for 30 min and the solvent removed under reduced pressure. Purification by silica gel chromatography eluting with 2:1 petroleum ether/EtOAc (0.5% AcOH) gave **7** as a bright-red solid (R_f=0.45, 242 mg, 82%); mp: (MeOH)=167.8–173.9 °C (dec.); ^{1}H NMR (300 MHz, [D_6]DMSO): δ=12.24 (br s, 1H), 3.16–2.91 (m, 2H), 2.57–2.36 (m, 14 H), 1.91–1.63 ppm (m, 2H); ^{13}C NMR (75 MHz, [D_6]DMSO): δ=174.6, 155.4, 147.0, 143.7, 131.7, 88.5, 34.4, 28.8, 27.0, 19.3, 16.7 ppm; ESI-MS $[M-H]^-$: m/z 585.0.

4-(4,4-Difluoro-2,6-diiodo-1,3,5,7-tetramethyl-4-bora-3a,4adiaza- s-indacene-8-yl)-butyric acid succinimidyl ester (**8**). A solution of compound **7** (100 mg, 0.17 mmol) in dry CH_3CN/DMF (2:1, 30 mL) under nitrogen was treated with NHS (29.4 mg, 0.26 mmol) and DCC (88 mg, 0.43 mmol). The reaction mixture was stirred overnight at room temperature and the solvent removed under reduced pressure. CH_2Cl_2 (30 mL) was added to the residue, which was washed with H_2O (3×10 mL), brine (2×10 mL), dried over Na_2SO_4 and concentrated to dryness. The crude solid was triturated with cold CH_3CN, filtered over a short silica plug and concentrated to dryness. Purification by silica gel chromatography eluting with 98:2 $CHCl_3$/MeOH gave **8** as a red solid (R_f=0.50, 91 mg, 78%); mp: (hexane/EtOAc)=199.1–203.4 °C (dec.); ^{1}H NMR (300 MHz, $CDCl_3$): δ=3.21–3.15 (m, 2H), 2.88–2.75 (m, 6H), 2.61 (s, 6H), 2.49 (s, 6H), 2.22–1.95 ppm (m, 2H); ^{13}C NMR (75 MHz, $CDCl_3$): δ=169.1, 167.8, 156.0, 143.8, 142.5, 131.5, 87.0, 30.9, 27.9, 26.1, 25.7, 19.2, 16.3 ppm; ESI-MS $[M-H]^-$: m/z 682.1.

4-(4,4-Difluoro-2,6-diiodo-1,3,5,7-tetramethyl-4-bora-3a,4adiaza- s-indacen-8-yl)-N-(3-(p-tolylamino)propyl)butanamide (**2**). A solution of compound 8 (80 mg, 0.106 mmol) in dry CH2Cl2/DMF (1:1, 15 mL) under nitrogen was treated with N1-(p-tolyl)propane- 1,3-diamine **9** (17.4 mg, 0.106 mmol). The reaction mixture was stirred overnight at room temperature and the solvent removed under reduced pressure. Purification by silica gel chromatography eluting with 96:4 CH_2Cl_2/MeOH gave 2 as a bright-red solid (R_f= 0.30, 45 mg, 58%); mp: (hexane/EtOAc)=187.2–189.3 °C (dec.); ^{1}H NMR (300 MHz, $CDCl_3$): δ=6.98 (d, J=8.0 Hz, 2H), 6.58 (d, J= 8.4 Hz, 2H), 3.32 (t, J=6.7 Hz, 2H), 3.14 (t, J=6.5 Hz, 2H), 3.09–3.00 (m, 2H), 2.61 (s, 6H), 2.49 (s, 6H), 2.34 (t, J=7.0 Hz, 2H), 2.22 (s, 3H), 2.00–1.86 (m, 2H), 1.79 ppm (quint, J=6.5 Hz, 2H); ^{13}C NMR (75 MHz, $CDCl_3$): δ=172.5, 155.4, 145.6, 145.2, 142.6, 131.4, 129.7, 127.2, 113.5, 86.5, 41.8, 37.3, 35.8, 28.6, 28.3, 27.3, 20.2, 18.8, 16.0 ppm; ESI-HRMS $[M+H]^+$: 733.0872, $C_{27}H_{34}BF_2I_2N_4O$ requires 733.0878; HPLC purity .95% (CH_3CN/H2O TFA 0.1% 80:20 (v/v), flow=1.0 mLmin^{-1}, t_R=6.0 min) at 226, 254, 390 and 526 nm.

Instrumentation

UV/vis absorption and fluorescence spectra were recorded with a Jasco V 650 spectrophotometer and a Fluorolog-2 (Model, F111) spectrofluorimeter, respectively. Fluorescence lifetimes were recorded with Fluorolog-2 (Model, F111) spectrofluorimeter equipped with a TCSPC Triple Illuminator. Solutions were excited by a Nanoled pulsed diode excitation source at 455 nm. The system measured fluorescence lifetimes with a resolution >200 ps. $^1O_2$ emission was registered with a Fluorolog-2 (Model, F111) spectrofluorimeter equipped with a NIR-sensitive liquid nitrogen cooled photomultiplier, exciting the air-equilibrated samples at 524 nm with the fluorimeter lamp.

Laser flash photolysis. All solutions were excited with the second harmonic of Nd-YAG Continuum Surelite II-10 laser (532 nm, 6 ns FWHM), using quartz cells with path length 1.0 cm. The excited solutions were analyzed with a Luzchem Research mLFP-111 apparatus with an orthogonal pump/probe configuration. The probe source was a ceramic xenon lamp coupled to quartz fiber-optic cables. The laser pulse and the mLFP-111 system were synchronized by a Tektronix TDS 3032 digitizer, operating in pre-trigger mode. The signals from a compact Hamamatsu photomultiplier were initially captured by the digitizer and then transferred to a personal computer, controlled by Luzchem Research software operating in the National Instruments LabView 5.1 environment. The solutions were deoxygenated by bubbling with a vigorous and constant flux of pure nitrogen (previously saturated with solvent). The solution temperature was 295±2 K. The energy of the laser pulse was measured at each shot with a SPHD25 Scientech pyroelectric meter.

Determination of fluorescence, 1O2 and triplet quantum yields

Fluorescence quantum yields were determined using optically matched solutions at the excitation wavelength of compounds 1 and 2 and a solution of Fluorescein in EtOH as standard (Φ_f= 0.79)[53] through the following Equation (1):

$$\Phi_f = \Phi_{f\,(s)} (In^2/I_{(s)}n^2_{(s)}) \quad (1)$$

where $\Phi_{f\,(s)}$ is the fluorescence quantum yield of the standard; I and I(s) are the areas of the fluorescence spectra of compounds and standard, respectively; n and n(s) are the refraction index of the solvents used for compounds and standard. Absorbance at the excitation wavelength was less than 0.1 in all cases. $^1O_2$ quantum yields were determined using optically matched solutions at the excitation wavelength of compounds 1 and 2, and Rose Bengal in acetonitrile as standard (Φ_Δ=0.65).[54] The values of Φ_Δ were determined from the following Equation (2):

$$\Phi_\Delta = \Phi_{\Delta(s)} (I/I_{(s)}) \quad (2)$$

where $\Phi_{\Delta(s)}$ is the $^1O_2$ quantum yield of the standard, I and I(s) are the areas of the fluorescence spectra of compounds and standard, respectively.
The relative quantum yields for the triplet formation were determined using optically matched solutions at the excitation wavelength of **1** and **2**. The top ΔA of the triplet signal from each solution was plotted as a function of the laser intensity. In this case, the initial part of each set of data points is proportional to the product $\Phi_T \times \varepsilon_{T\text{-}T}$, where Φ_T and $\varepsilon_{T\text{-}T}$ are the quantum yield of the triplet state and its molar absorption coefficient, respectively. Assuming very similar values for the triplet state of the BODIPY chromophores for 1 and 2, the relative Φ_T values were estimated directly by the different slopes (π) of the straight lines obtained from the linear portion of the plots via the simple Equation (3)

$$\Phi_T = \Phi_{T(s)}\, \pi / \pi_{(s)} \quad (3)$$

Nitric oxide detection
NO release was measured with a World Precision Instrument, ISONO meter, equipped with a data acquisition system, and based on direct amperometric detection of NO with short response time (< 5 s) and sensitivity range 1 nm–20 mm. The analog signal was digitalized with a four-channel recording system and transferred to a computer. The sensor was accurately calibrated by mixing standard solutions of $NaNO_2$ with 0.1m H_2SO_4 and 0.1m KI according to the reaction:

$$4H^+ + 2I^- + 2NO_2^- \rightarrow 2H_2O + 2NO + I_2$$

Irradiation was in a quartz cell (1 cm path length, 3 mL capacity) by 200 mW continuum lasers with λexc=405 nm and 532 nm. NO measurements were carried out under stirring with the electrode positioned outside the light path, to avoid NO signal artefacts due to photoelectric interference on the ISO-NO electrode.

Confocal fluorescence microscopy

Fluorescence confocal imaging was performed on an inverted Nikon Ti-E microscope (Nikon Co., Shinjuku, Japan). The confocal fluorescence microscope Nikon A1 is equipped with an Argon ion CW laser and 405 nm and 485 nm pulsed/CW diode lasers (Pico- Quant GmbH, Berlin, Germany). Images of 1024O1024 pixels were collected using a Nikon Plan Apo VC 60 oil-immersion objective with NA 1.40. Filters were set to register the DAPI fluorescence ofcells in the 425–475 nm range and the fluorescence of the BODIPY dye in the 500–550 nm or 570–620 nm range.

Experiments in vitro

A375 cell line, obtained from American Type Culture Collection (Rockville, MD, USA), was maintained in Dulbecco's modified Eagle's medium (DMEM) containing 10% fetal calf serum (FCS), 2.0 mm l-glutamine, 100 UmL^{-1} penicillin, 100 mgmL¢1 streptomycin, and 25 $mgmL^{-1}$ fungizone (Sigma–Aldrich, Italy), and incubated at 37 °C in a humidified atmosphere containing 5% CO_2, following the procedure reported elsewhere.[55] Cells from confluent cultures were detached using trypsin/EDTA and seeded in complete DMEM. For cell staining, the cells were cultured in 12-well culture dishes for 24 h. The medium was removed and replaced with medium without phenol red, containing the sample solution, for 4 h. The cells were first washed with PBS, then fixed with 4% formaldehyde. After washing with PBS, cells were incubated with 4,6-diamino-2- phenylindole (DAPI, 1:10000; Invitrogen) for 10 min. Compounds **1** and **2** were dissolved in CH_3CN and slowly evaporated to form thin films. These were then hydrated with DMEM with 10% FCS without red phenol. The mixtures were stirred for 2 h at room temperature. The photocytotoxicity experiments were carried out by irradiating cells, incubated

without/with photoactive components, with RPR lamps with emission centered at λ=420 nm (~7 $mWcm^{-2}$) and 528 nm (~0.5 $mWcm^{-2}$) in a Rayonet photochemical reactor. Cell proliferation was assessed by MTT assays, based on the conversion of a substrate containing a tetrazolium ring to spectrophotometrically detectable formazan by mitochondrial dehydrogenases.[56] Briefly, cells were seeded at an initial density of 8×10^3 cells per microwell in flat-bottomed 200 mL microplates, and incubated at 37°C in a humidified atmosphere containing 5% CO_2 for 24 h. Subsequently, some cells were maintained as media controls, while others were incubated with the photoactive compounds. In both cases, complete DMEM without phenol red was used; 20mL of 0.5% 3-(4,5-dimethylthiazol-2-yl)2,5-diphenyltetrazolium bromide in PBS were then added to each microwell. Following 4 h of incubation at 37°C, the supernatant was removed and replaced with 100 μL of DMSO. The optical density of the contents of each well was measured with a microplate spectrophotometer reader (Digital and Analog Systems, Rome, Italy) at 550 nm. Cell viability (%) was calculated from the following Equation (4):

$$\text{Cell Viability (\%)} = [A_{\text{Before}} - (A_{\text{After}} / A_{\text{Before}})] \times 100 \qquad (4)$$

where A_{Before} and A_{After} are the absorbance values of the wells, treated with the sample solutions, respectively before and after irradiation.

Acknowledgements

We thank the Associazione Italiana per la Ricerca sul Cancro (AIRC), Project IG-12834, and the Ministero Istruzione Università e Ricerca (MIUR), PRIN 2011, and Ricerca Locale ex-60% from the University of Turin for financial support.

Keywords: bimodal therapy, light, nitric oxide, photodynamic therapy, radicals.

[1] M. Wainwright in Photosensitizers in Biomedicine, Wiley-Blackwell, 2009, pp. 213–233.
[2] P. Agostinis, K. Berg, K. A. Cengel, T. H. Foster, A. W. Girotti, S. O. Gollnick, S. M. Hahn, M. L. R. Hamblin, A. Juzeniene, D. Kessel, M. Korbelik, J. Moan, P. Mroz, D. Nowis, J. Piette, B. C. Wilson, J. Golab, CA-Cancer J. Clin. 2011, 61, 250–281.
[3] B. C. Wilson, M. S. Patterson, Phys. Med. Biol. 2008, 53, R61–109.
[4] A. P. Castano, T. N. Demidova, M. R. Hamblin, Photodiagn. Photodyn. Ther. 2004, 1, 279–293.
[5] A. P. Castano, T. N. Demidova, M. R. Hamblin, Photodiagn. Photodyn. Ther. 2005, 2, 91–106.
[6] R. Saavedra, L. B. Rocha, J. M. Da˛browski, L. G. Arnaut, ChemMedChem 2014, 9, 390–398.
[7] A. P. Castano, T. N. Demidova, M. R. Hamblin, Photodiagn. Photodyn. Ther. 2005, 2, 1–23.
[8] L. G. Arnaut, M. M. Pereira, E. F. F. Silva, F. A. Schaberle, A. R. Abreu, L. B. Rocha, M-M- Barsan, K-Urbanska, G. Stochel, C. M. A. Brett, Chem. Eur. J. 2014, 20, 5346–5357.
[9] D. Nowis, M. Makowski, T. Stokłosa, M. Legat, T. Issat, J. Gołab, Acta Biochim. Pol. 2005, 52, 339–352.
[10] B. Krammer, Anticancer Res. 2001, 21, 4271–4277.
[11] J. M. Da˛browski, L. G. Arnaut, Photochem. Photobiol. Sci. 2015, 14, 1765 – 1780.
[12] M. R. Hamblin, T. Hasan, Photochem. Photobiol. Sci. 2004, 3, 436–450.
[13] T. A. Maisch, Mini-Rev. Med. Chem. 2009, 9, 974–983.
[14] M. A. Biel in Photodynamic Therapy: Methods and Protocol. (Ed.: G. J. Gomer), Springer, 2010, pp. 175–194.
[15] M. R. Detty, S. L. Gibson, S. J. Wagner, J. Med. Chem. 2004, 47, 3897 – 3915.
[16] A. B. Ormond, H. S. Freeman, Materials 2013, 6, 817–840.
[17] M. Triesscheijn, P. Baas, J. H. M. Schellens, F. A. Stewart, Oncologist 2006, 11, 1034–1044.
[18] S. B. Brown, E. A. Brown, I. Walker, Lancet Oncol. 2004, 5, 497–508.
[19] S. H. Lim, C. Thivierge, P. Nowak-Sliwinska, J. Han, H. van der Bergh, G. WagniAres, K. Burgess, H. B. Lee, J. Med. Chem. 2010, 53, 2865–2874.
[20] T. Yogo, Y. Urano, Y. Ishitsuka, F. Maniwa, T. Nagano, J. Am. Chem. Soc. 2005, 127, 12162–12163.
[21] A. Loudet, K. Burgess, Chem. Rev. 2007, 107, 4891–4932.
[22] S. G. Awuah, Y. You, RSC Adv. 2012, 2, 11169–11183.
[23] A. Kamkaew, S. H. Lim, H. B. Lee, L. V. Kiew, L. Y. Chung, K. Burgess, Chem. Soc. Rev. 2013, 42, 77–88.
[24] A. E. O'Connor, M. M. McGee, Y. Likar, V. Ponomarev, J. J. Callanan, D. F. O'Shea, A. T. Byrne, W. M. Gallagher, Int. J. Cancer 2012, 130, 705–715.
[25] A. T. Byrne, A. E. O'Connor, M. Hall, J. Murtagh, K. O'Neill, K. M. Curran, K. Mongrain, J. A. Rousseau, R. Lecomte, S. McGee, J. J. Callanan, D. F. O'Shea, W. M. Gallagher, Br. J. Cancer 2009, 101, 1565–1573.
[26] J. F. Kerwin, Jr. , J. R. Lancaster, P. L. Feldman, J. Med. Chem. 1995, 38, 4343–4362.

[27] A. A. Noronha-Dutra, M. M. Epperlein, N. Woolf, FEBS Lett. 1993, 321, 59–62.
[28] W. A. Pryor, G. L. Squadrito, Am. J. Physiol. 1995, 268, L699–722.
[29] C. Ratanatawanate, A. Chyao, K. J. Balkus, Jr., J. Am. Chem. Soc. 2011, 133, 3492–3497.
[30] D. Fukumura, S. Kashiwagi, R. K. Jain, Nat. Rev. Cancer 2006, 6, 521–534.
[31] L. A. Ridnour, D. D. Thomas, S. Donzelli, M. G. Espey, D. D. Roberts, D. A. Wink, J. S. Isenberg, Antioxid. Redox Signaling 2006, 8, 1329–1337.
[32] J. R. Hickok, D. D. Thomas, Curr. Pharm. Des. 2010, 16, 381–391.
[33] C.-F. Chang, A. R. Diers, N. Hogg, Free Radical Biol. Med. 2015, 79, 324 – 336.
[34] P. G. Wang, M. Xian, X. Tang, X. Wu, Z. Wen, T. Cai, A. J. Janczuk, Chem. Rev. 2002, 102, 1091–1134.
[35] A. W. Carpenter, M. H. Schoenfisch, Chem. Soc. Rev. 2012, 41, 3742.
[36] J. Lehmann, Expert Opin. Ther. Pat. 2000, 10, 559–574.
[37] S. J. Wimalawansa, Expert Opin. Pharmacother. 2008, 9, 1935–1954.
[38] T. B. Cai, G. Wang, Expert Opin. Ther. Pat. 2004, 14, 849–857.
[39] S. Huerta, S. Chilka, B. Bonavida, Int. J. Oncol. 2008, 33, 909–927.
[40] B. Bonavida, S. Baritaki, S. Huerta-Yepez, M. I. Vega, D. Chatterjee, K. Yeung, Nitric Oxide 2008, 19, 152–157.
[41] See, for example: a) S. Sortino, Chem. Soc. Rev. 2010, 39, 2903–2913; b) P. C. Ford, Acc. Chem. Res. 2008, 41, 190–200; c) N. L. Fry, P. K. Mascharak, Acc. Chem. Res. 2011, 44, 289–298; d) P. C. Ford, Nitric Oxide 2013, 34, 56–64.
[42] E. B. Caruso, S. Petralia, S. Conoci, S. Giuffrida, S. Sortino, J. Am. Chem. Soc. 2007, 129, 480–481.
[43] S. Conoci, S. Petralia, S. Sortino (STMicroelectronics, S.r.l.), Eur. Pat. No. EP2051935A1, 2006.
[44] See, for example: a) A. Fraix, N. Kandoth, I. Manet, V. Cardile, A. C. E. Graziano, R. Gref, S. Sortino, Chem. Commun. 2013, 49, 4459–4461; b) N. Kandoth, E. Vittorino, M. T. Sciortino, I. Colao, A. Mazzaglia, S. Sortino, Chem. Eur. J. 2012, 18, 1684–1690; c) N. Kandoth, V. Kirejev, S. Monti, R. Gref, M. B. Ericson, S. Sortino, Biomacromolecules 2014, 15, 1768–1776; d) C. Fowley, A. P. McHale, B. McCaughan, A. Fraix, S. Sortino, J. F. Callan, Chem. Commun. 2015, 51, 81–84.
[45] T. Suzuki, O. Nagae, Y. Kato, H. Nakagawa, K. Fukuhara, N. Miyata, J. Am. Chem. Soc. 2005, 127, 11720–11726.
[46] K. Kitamura, N. Ieda, K. Hishikawa, T. Suzuki, N. Miyata, K. Fukuhara, H. Nakagawa, Bioorg. Med. Chem. Lett. 2014, 24, 5660–5662.
[47] A. Fraix, S. Guglielmo, V. Cardile, A. C. E. Graziano, R. Gref, B. Rolando, R. Fruttero, A. Gasco, S. Sortino, RSC Adv. 2014, 4, 44827–44836.
[48] W. Wu, H. Guo, W. Wu, S. Ji, J. Zhao, J. Org. Chem. 2011, 76, 7056–7064.
[49] S. Monti, I. Manet, Chem. Soc. Rev. 2014, 43, 4051–4067.
[50] D. Wang, J. Fan, X. Gao, B. Wang, S. Sun, X. Peng, J. Org. Chem. 2009, 74, 7675–7683.
[51] F. L. Callari, S. Sortino, Chem. Commun. 2008, 1971–1973.
[52] L. R. Orelli, M. B. Garcia, F. Niemevz, I. A. Perillo, Synth. Commun. 1999, 29, 1819–1833.
[53] R. E. Kellogg, R. G. Bennett, J. Chem. Phys. 1964, 41, 3042.
[54] S. Mathai, T. A. Smith, K. P. Ghiggino, Photochem. Photobiol. Sci. 2007, 6, 995–1002.
[55] V. Cardile, G. Malaponte, C. Loreto, M. Libra, S. Caggia, F. M. Trovato, G. Musumeci, Acta Histochem. 2013, 115, 795–802.
[56] R. Parenti, V. Cardile, A. C. Graziano, C. Parenti, A. Venuti, M. P. Bertuccio, D. L. Furno, G. Magro, PLoS One 2014, 9, e114333.